Expanded View Figures

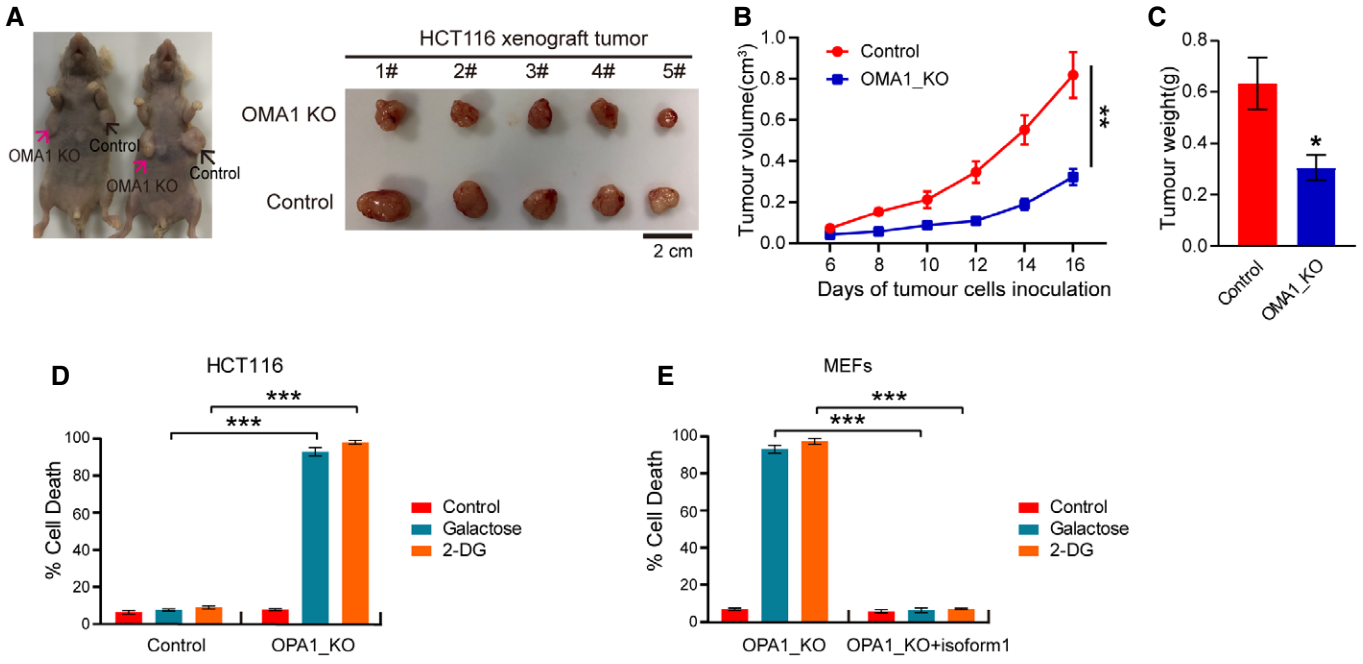

Figure EV1. Loss of OMA1 significantly reduced colorectal tumor growth in nude mice and OPA1 deficiency makes cells more dependent on glycolysis for survival.

A–C Control or OMA1 KO HCT116 cells (5×10^6) were injected into the flanks of nude mice. Mice were euthanized and photographed at day 16 (A). Representative photographs of tumors in nude mice were performed (A) and tumor weights were analyzed (C). The tumor sizes were measured at an interval of 6 days after injection and calculated as = width^2 × length/2. Xenograft tumor growths of control or OMA1 KO HCT116 tumors in nude mice were shown (B). Data are presented as the mean ± SEM, $n = 5$ biological replicates. Scale bars, 2 cm. *P*-values were calculated by two-way ANOVA of variance; $^*P < 0.05$, $^{**}P < 0.01$. All experiments were repeated with three independent biological replicates.

D Control and OPA1 KO HCT116 cells were treated with glucose deprivation (galactose) or the glycolytic inhibitor (2-Deoxy-D-glucose, 2-DG, 10 mM) for 24 h. Cell deaths were quantified by cell counting with trypan blue exclusion. Error bars represent the mean ± SD ($n = 3$, 300 cells per independent experiment), statistical significance was assessed by a two-way ANOVA of variance, $^{***}P < 0.001$.

E OPA1-null MEFs expressing control (empty vector) or OPA1 isoform 1 were cultured with galactose or 2-DG for 48 h. Cell death was quantified by cell counting with trypan blue exclusion. Error bars represent the mean ± SD ($n = 3$, 300 cells per independent experiment), statistical significance was assessed by a two-way ANOVA of variance, $^{***}P < 0.001$.

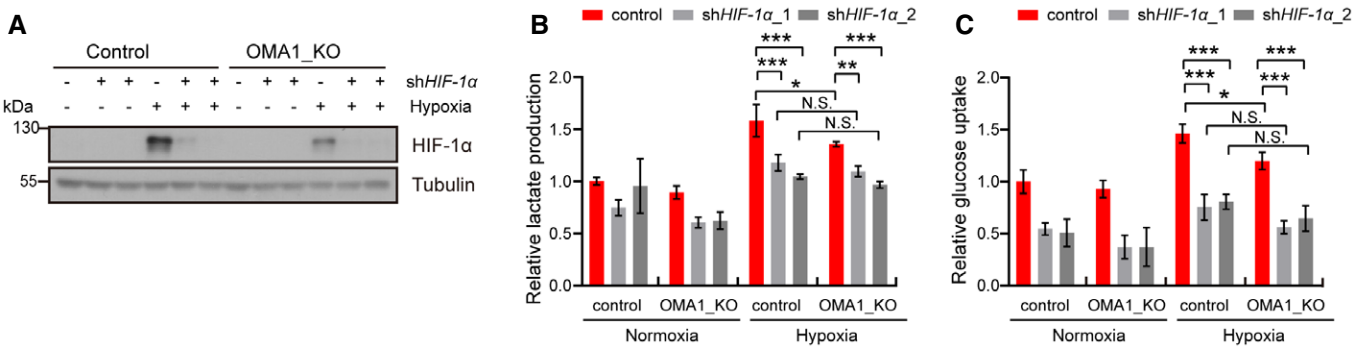

Figure EV2. OMA1 regulates glycolysis in a HIF-1α dependent manner.

A–C Control or OMA1_KO HCT116 cells were transfected with control, sh*HIF-1α*_1, or sh*HIF-1α*_2 (*HIF-1α* knockdown) lentiviral particles. And cells were cultured in normoxia or hypoxia for 12 h. The whole cell lysates were analyzed by Western blotting with antibodies against HIF-1α, Tubulin (representative data from three independent experiments) (A). The lactate production (B) and glucose uptake (C) were measured using microplate reader, and the values were normalized to the protein concentration. Error bars indicate the mean ± SD ($n = 4$ independent experiments), statistical significance was assessed by a two-way ANOVA. N.S., not significant, *$P < 0.05$, ***$P < 0.001$.

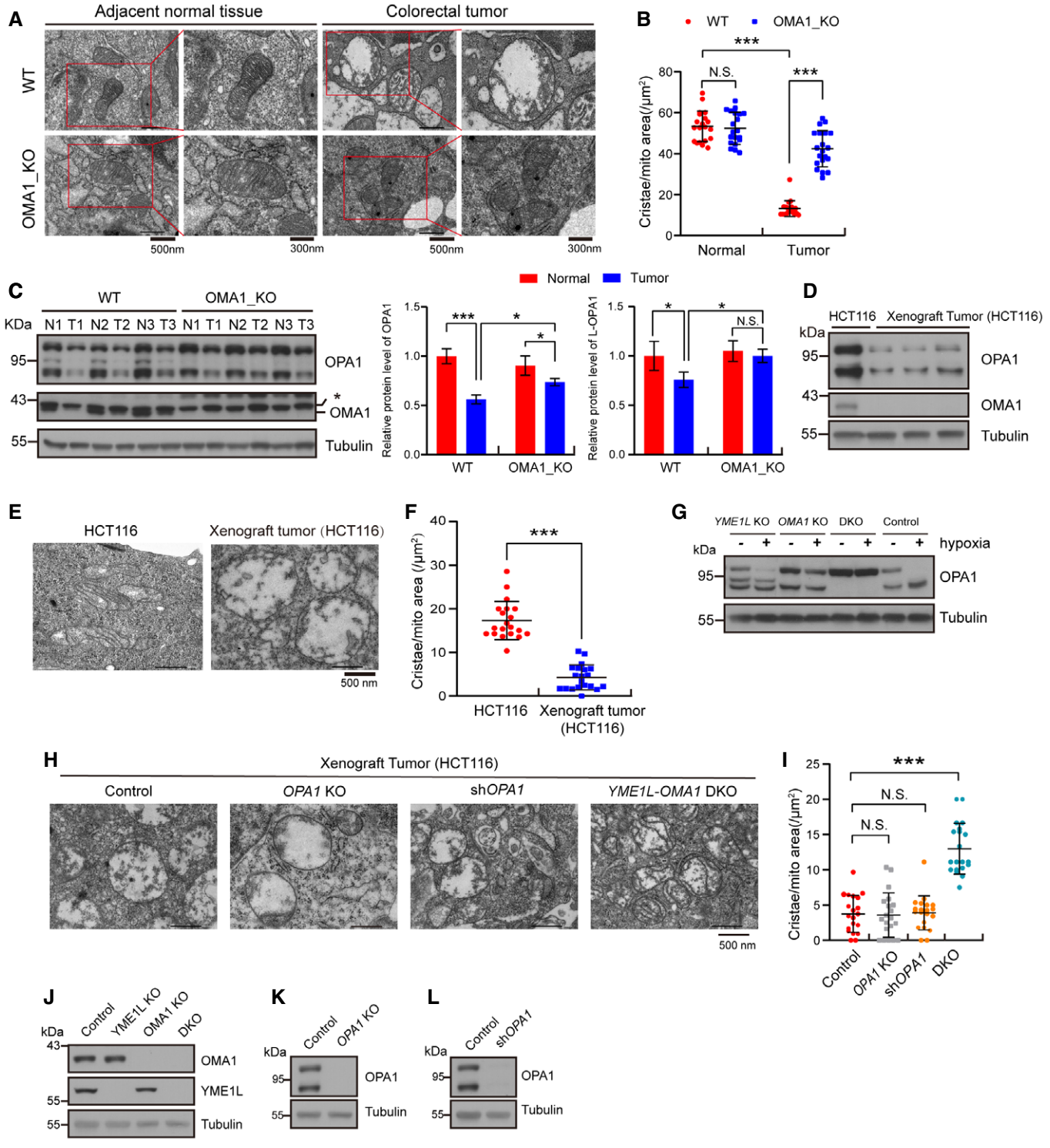
A
Adjacent normal tissue
Colorectal tumor
WT
OMA1_KO
500nm
300nm
500nm
300nm
B
WT
OMA1_KO
***
N.S.
***
Cristae/mito area(/μm²)
Normal
Tumor
C
WT
OMA1_KO
KDa
N1 T1 N2 T2 N3 T3 N1 T1 N2 T2 N3 T3
95
43
55
OPA1
*
OMA1
Tubulin
Normal
Tumor
Relative protein level of OPA1
Relative protein level of L-OPA1
WT
OMA1_KO
D
HCT116
Xenograft Tumor (HCT116)
kDa
95
43
55
OPA1
OMA1
Tubulin
E
HCT116
Xenograft tumor (HCT116)
500 nm
F
Cristae/mito area (/μm²)
HCT116
Xenograft tumor (HCT116)
G
YME1L KO
OMA1 KO
DKO
Control
hypoxia
kDa
95
55
OPA1
Tubulin
H
Xenograft Tumor (HCT116)
Control
OPA1 KO
shOPA1
YME1L-OMA1 DKO
500 nm
I
Cristae/mito area(/μm²)
N.S.
N.S.
Control
OPA1 KO
shOPA1
DKO
J
kDa
Control
YME1L KO
OMA1 KO
DKO
43
55
55
OMA1
YME1L
Tubulin
K
kDa
Control
OPA1 KO
95
55
OPA1
Tubulin
L
kDa
Control
shOPA1
95
55
OPA1
Tubulin

Figure EV3.

Figure EV3. OMA1-OPA1 axis regulates mitochondrial cristae remodeling of colorectal cancer cells *in vivo*.

A Representative transmission electron microscopy (TEM) analysis of the colorectal tumors or adjacent normal tissues from WT or *Oma1*$^{-/-}$ mice.

B Quantitative analysis of mitochondrial cristae (the ratio of cristae number to mitochondrial area) in tumor or adjacent normal tissues from WT and *Oma1*$^{-/-}$ mice (20 mitochondria per group, biological replicates). Statistical significance was assessed by a two-way ANOVA; error bars are presented as mean ± SD; N.S., not significant, ***$P < 0.001$.

C The lysates of the adjacent normal tissues or tumors from WT and *Oma1*$^{-/-}$ mice were stained with antibodies against OPA1, OMA1, or Tubulin (representative data from three independent experiments). The asterisk indicates a nonspecific band. The bands of OPA1 and L-OPA1 were further quantified by ImageJ software. Error bars indicate the mean ± SD ($n = 3$ independent experiments), statistical significance was assessed by two-way ANOVA. N.S., not significant, *$P < 0.05$, ***$P < 0.001$.

D The lysates of HCT116 cells or xenograft tumor of nude mice injected with HCT116 cells were assessed by Western blotting with anti-OPA1, or anti-OMA1, or anti-Tubulin (representative data from three independent experiments).

E Representative TEM analysis of HCT116 cells or the xenograft tumors of nude mice injected with HCT116 cells.

F Quantitative analysis of mitochondrial cristae (the ratio of cristae number to mitochondrial area) in HCT116 cells or the xenograft tumors of nude mice injected with HCT116 cells (20 mitochondria per group, biological replicates). Statistical significance was assessed by Student's *t*-test; error bars are presented as mean ± SD; ***$P < 0.001$.

G *YME1L*_KO, *OMA1*_KO, *YME1L_OMA1*_Double KO (DKO), and WT HCT116 cells were maintained in normoxia or hypoxia (1% O_2) for 72 h. The whole cell lysates were analyzed by Western blotting with antibody against OPA1. Tubulin was used as a loading control.

H, I Representative TEM analyzed the inside of the xenograft tumors from nude mice injected with control, *OPA1*_KO, sh*OPA1*, *YME1L-OMA1-DKO* HCT116 cells (H). Quantitative analysis of mitochondrial cristae (the ratio of cristae number to mitochondrial area) was further performed (I) (20 mitochondria per group, biological replicates). Statistical significance was assessed by a two-way ANOVA; error bars are presented as mean ± SD; N.S., not significant, ***$P < 0.001$.

J WT, *YME1L*_KO, *OMA1*_KO, and *YME1L_OMA1*_Double KO (DKO) HCT116 cells were analyzed by Western blotting with antibodies against OMA1, YME1L, and Tubulin.

K, L Control and *OPA1*_KO (K), Control and sh*OPA1* (L) HCT116 cells were analyzed by Western blotting with antibodies against OPA1 and Tubulin.

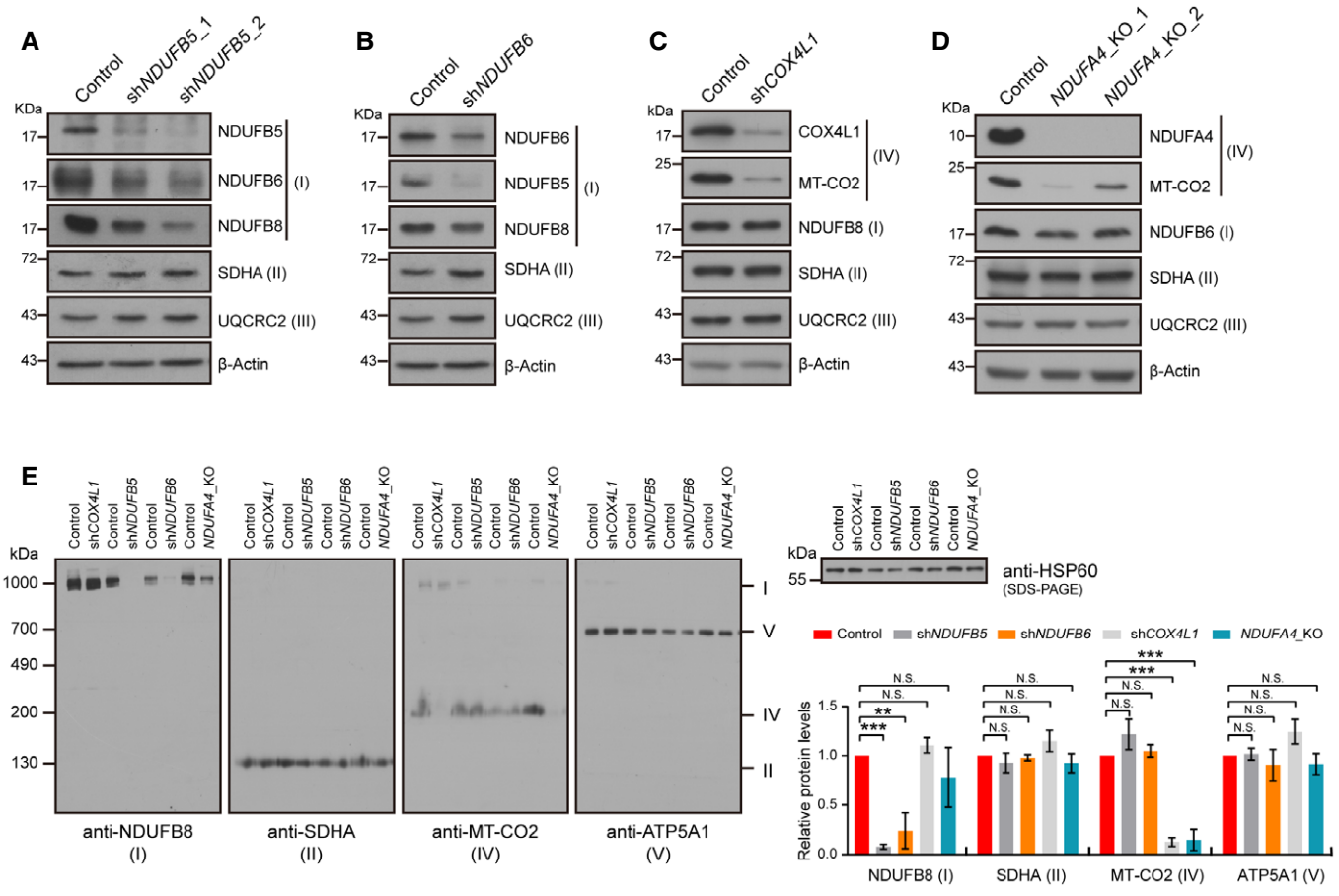

Figure EV4.

Figure EV4. Depletion of NDUFB5, NDUFB6, COX4L1, or NDUFA4 impairs the assembly of mitochondrial respiratory chain complexes.

A HCT116 cells were transfected with control, sh*NDUFB5*_1 or sh*NDUFB5*_2 (*NDUFB5* knockdown) lentiviral particles, and the cell lysates were assessed by Western blotting with anti-NDUFB5, anti-NDUFB6, anti-NDUFB8, anti-SDHA, anti-UQCRC2, or anti-β-Actin. (representative data from three independent experiments).

B HCT116 cells infected with control or sh*NDUFB6* (*NDUFB6* knockdown) lentiviral particles were lysed and analyzed by Western blotting with antibodies against NDUFB5, NDUFB6, NDUFB8, SDHA, UQCRC2, or β-Actin. (representative data from three independent experiments).

C HCT116 cells were transfected with control or sh*COX4L1* (*COX4L1* knockdown) lentiviral particles and the cell lysates were assessed by Western blotting with anti-COX4L1, anti-MT-CO2, anti-NDUFB8, anti-SDHA, anti-UQCRC2, or anti-β-Actin. (representative data from three independent experiments).

D Western blotting analysis of HCT116 control or *NDUFA4* KO (*NDUFA4* knockout) cell lysates with antibodies against NDUFA4, MT-CO2, NDUFB6, SDHA, UQCRC2, or β-Actin. (representative data from three independent experiments).

E Mitochondria isolated from control and sh*COX4L1*, control and sh*NDUFB5*, control and sh*NDUFB6*, control and *NDUFA4*_KO HCT116 cells were subjected to blue native PAGE (BN-PAGE), and respiratory chain complexes were analyzed by Western blotting with anti-NDUFB8 (Complex I), anti-SDHA (Complex II), anti-MT-CO2 (Complex IV), and anti-ATP5A1 (Complex V, ATP synthase) antibodies. SDS–PAGE with antibody against HSP60 was used as a loading control. Relative protein levels were further evaluated by densitometry analysis using ImageJ software. Error bars are presented as mean ± SD by Student's *t*-test ($n = 3$ independent experiments). N.S., not significant, $^{**}P < 0.01$, $^{***}P < 0.001$.

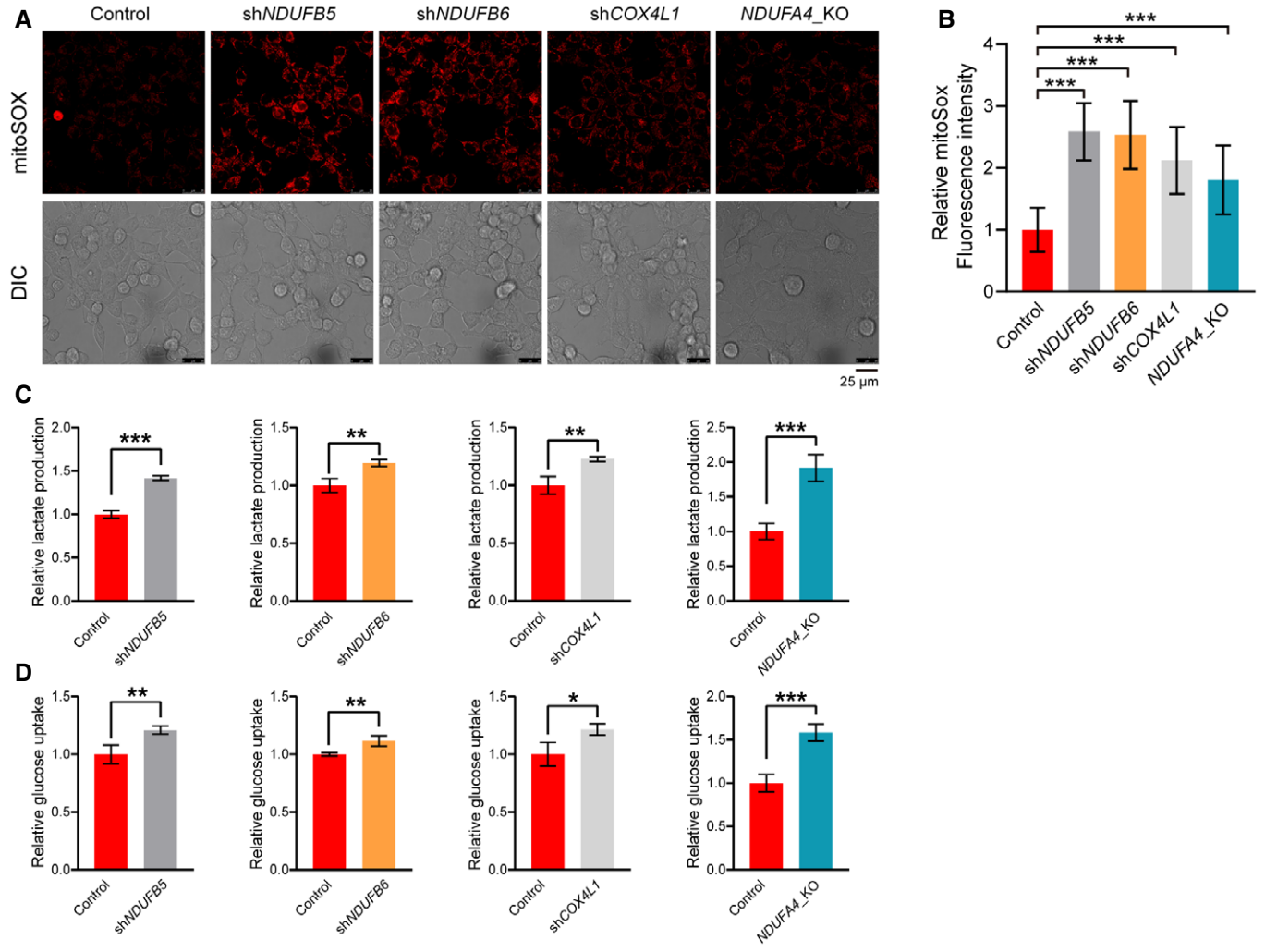

Figure EV5.

Figure EV5. Mitochondrial respiratory chain complexes component NDUFB5, NDUFB6, COX4L1, or NDUFA4 regulates mtROS generation and glycolytic metabolism.

A, B Control, sh*COX4L1*, sh*NDUFB5*, sh*NDUFB6*, and *NDUFA4*_KO HCT116 cells were stained with mitoSOX and then analyzed by confocal microscopy (A). The fluorescence intensities of mitoSOX were analyzed by ImageJ software (B). Bars indicate the mean ± SD of three independent experiments by Student's *t*-test, ***$P < 0.001$.

C, D Control and sh*COX4L1*, control and sh*NDUFB5*, control and sh*NDUFB6*, control and *NDUFA4*_KO HCT116 cells were cultured for 24 h. The lactate production (C) and glucose uptake (D) were measured by using microplate reader, and the values were normalized to the protein concentration. Error bars indicate the mean ± SD ($n = 3$ independent experiments), statistical significance was assessed by *t*-test, *$P < 0.05$, **$P < 0.01$, ***$P < 0.001$.

